Poly(vinyl alcohol) and Functionalized Ionic liquid Based Smart Hydrogel for Doxorubicin Release

Muzammil Kuddushi,[a,c] Debes Ray,[b] Vinod Aswal,[b] Clare Hoskins,[c*] Naved Malek[a*]

[a]Applied Chemistry Department, S.V. National Institute of Technology, Surat-395007, Gujarat, India.
[b]Solid State Physics Division, Bhabha Atomic Research Center Trombay, Mumbai 400085 (India)

[c]Department of Pure & Applied Chemistry, University of Strathclyde, 99 George Street, Glasgow, UK.

*Corresponding authors E-mails: navedmalek@yahoo.com, navedmalek@chem.svnit.ac.in, clare.hoskins@strath.ac.uk

ABSTRACT

Limitations associated with the traditional cancer therapies prompt the scientific community to develop an effective, safer, smarter and targeted drug carriers that improve the efficiency of the drug carrier, reduce the adverse effects of the drug on the healthy cells, and helps in preventing the cancer recurrences. This research aims to design a stimuli-responsive, self-healable, adhesive, and injectable polymeric hydrogel with ester functionalized ionic liquid (ILs) as one of the additives to improve the efficiency of the anti-cancer drug in encapsulation and localized delivery. The designed polymeric hydrogel responds to intracellular biological stimuli (e.g. acidic pH of cancerous cells and temperature), change the morphology through changing the shape and size of the gelator within the hydrogel matrix and release the encapsulated doxorubicin (DOX) at the tumor site efficiently. Molecular interactions, gel morphology, and mechanical strength of the hydrogel were characterized through various analytical techniques, including small angle neutron scattering (SANS). Adhesive properties of the polymeric hydrogel were measured by lap-shear strength tests and biocompatibility and cellular drug uptake study on human breast cancer (MCF-7) and human cervical carcinoma cells (HeLa). *The in-vitro* cytotoxicity and drug release study showed that the hybrid hydrogel is more effective at killing the cancerous cells, and the targeted release of the DOX occurred at intracellular acidic pH. The polymeric hydrogel provides an efficient therapeutic approach for the encapsulation and release of the drug. Overall, the study offers a proof of

concept to test the feasibility of the hydrogel system whether the hydrogel formulation helped or hindered the total cellular DOX trafficking.

Keywords: Injectable hydrogel; Self-healable gel; stimuli responsive drug release; localized chemotherapy; cancer recurrence.

1. Introduction

Cancer is causing ~9.6 million deaths globally in 2018 (second highest after heart disease) with 1 in 6 deaths is due to cancer. Abnormal cell proliferation and metastasis that leads to cancer development and recurrence after treatment and results in the above statastics.[2,3] Surgical removal of the cancerous cells are normally followed by a round of chemotherapy or radiotherapy in order to lower the expectancy of tumor metastasis.[4] Doxorubicin (DOX) is an approved chemotherapeutic drug for the treatment of lung, breast, ovarian, and acute lymphoblastic leukaemia.[5] However, clinical application of DOX is hindered by its dose-dependent non-site-specific toxicity, such as cardio-toxicity and prevalence of off target effects. Several drug carriers have recently been studied to carry the drug molecules for the site-specific delivery such as liposomes, niosomes, solid lipid nanoparticles, polymeric micelles, dendrimers, nanotubes, and magnetic nanoparticles. These carriers reduce the drug administration dosages needed for treatment and are cost-effective. They also reduce the severe systematic off target side effects experienced through intravenous administration.[6] But these carriers suffer from instability in circulation, poor batch-to-batch reproducibility, poor oral bioavailability, difficulty with sterilization, poor drug solubility, and accompanied toxicity to name a few.[7,8] These can be overcome through site-specific stimuli responsive localized drug delivery.

Stimuli responsive polymeric hydrogels are among the well-recognized and recently tested site-specific drug carriers.[9] However, they suffer lower mechanical strength, rapid but limited drug loading, poor physical stability, non-injectability, non-biodegradability and potential toxicity.[10,11] These could be improved through incorporating external additives and modified solution

conditions.[12] Thermo-responsive polymeric hydrogel synthesized by Qu et al through free radical polymerization exhibited increased drug release from the hydrogel matrix with rise in the temperature. Increasing the temperature of the hydrogel through irradiation decrease the mesh size and increases the release of loaded drug molecules. The gold nanorods (GNRs) doped DOX loaded polymeric hydrogel prevented the breast cancer recurrence effectively and efficiently than the undoped DOX loaded polymeric hydrogel after primary tumor resection.[13]

New advancements in localized chemotherapy have led to design smart switchable hydrogel system that enable further control over the physicochemical behavior of the gel matrix, which is highly desirable in the site-specific delivery of chemotherapies and are stimuli- responsive, which response to different stimuli or changes in the physiochemical environment i.e. pH, electric field, temperature, magnetic fields, light intensity and biological molecules to name a few.[14-16] The hydrogels undergo changes in their several physicochemical properties such as colour or transparency, conductivity, permeability and phase behavior on account of the external stimuli. [14-16]

In our quest towards smart drug carriers for the targeted drug delivery, we had tested various soft assemblies including vesicles, coacervates and hydrogels for their ability to transport the drug molecules.[17-22] In continuation to that, herein we report poly(vinyl alcohol) (PVA) based hybrid hydrogel consisting of ester functionalized morpholinium based ionic liquid ($C_{16}EMorphBr$) and other biocompatible additives including, dextrose, glycerol and sodium tetraborate. The polymeric hydrogel is stimuli responsive hybrid, biocompatible, biodegradable and high drug uptake efficient delivery system with ability to self-healing **(Scheme 1)**. PVA is a known water soluble, biocompatible, biodegradable and thermo-responsive polymer that has been used in numerous biomedical applications including in implants, contact lenses, drug delivery devices, artificial heart surgery, in repairing and regenerating tissues and organs and wound dressings.[23,24] Biocompatible and biodegradable (4-(2-(hexadecyloxy)-2-oxoethyl)-4-methylmorpholin-4-ium bromide ($C_{16}EMorphBr$) was added to modulate the properties of the PVA through synergistic interactions.[25,26] It was observed that drug encapsulation and loading capacity

was improved in the presence of C_{16}EMorphBr. The presence of an oxygen atom in the morpholine ring and the cleavable ester functional group in the long alkyl chain (hydrophobic part) significantly increases the biocompatibility and biodegradability (ester hydrolysis by its (−I) effect) of the IL.[27] The hydrophobic alkyl chains of the C_{16}EMorphBr through hydrophobic interactions with the polymeric chains of the PVA forms 3D network structure that can carry the doxorubicin (DOX) within the gel network. Introducing dextrose and glycerol enhances the mechanical properties whereas sodium tetraborate introduces the self-healing property within the hydrogel matrix. Overall our prime objective is to construct a self-assembled structure that is capable of not only encapsulating anti-cancer drugs but also is site specific and possesses stimuli-responsive properties with biodegradable, biocompatible, adhesive and self-healing characteristics.
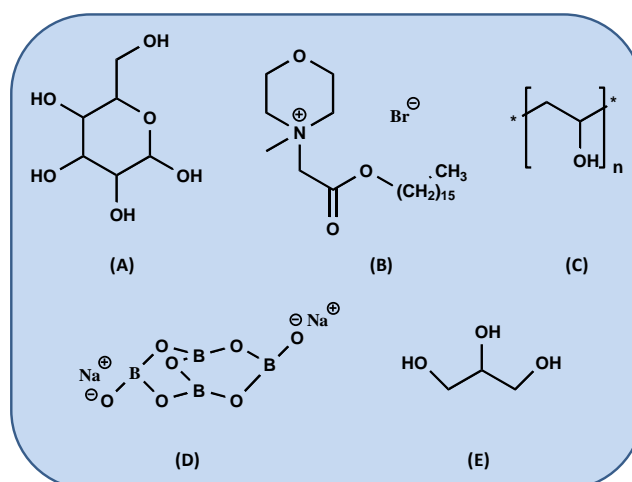
Scheme 1. Chemical structures of (A) Dextrose, (B) C_{16}EMorphBr, (C) PVA, (D) Sodium tetra borate and (E) Glycerol.

2. Experimental Section

2.1 Materials

Poly(vinyl alcohol) (PVA), dextrose (≥99.5%), glycerol (≥99.0%) and sodium tetraborate (99.98%) were used as received from Sigma Aldrich. (4-(2-

(hexadecyloxy)-2-oxoethyl)-4-methylmorpholin-4-ium bromide(C_{16}EMorphBr) was synthesized and characterized according to the reported procedure.[26]

2.2 Preparation of the hydrogel

PVA (5000 mg), dextrose (250 mg), C_{16}EMorphBr (500 mg), and glycerol (2.52 mL) were mixed in deionized water (75 mL), heated in a water bath at 70 °C for 90 min to form a transparent solution. The solution was then cooled to room temperature and mixed with sodium tetraborate solution (25 mL, 0.04 mol L^{-1}). The resulting mixture was then heated with stirring at 75 °C in water bath for 60 min giving a homogeneous transparent solution. The mixture when cooled to room temperature forms the polymeric transparent hydrogel **(Scheme 2)**. The resulting hydrogel have PVA (580 mM), C_{16}EMorphBr (11 mM), dextrose (13 mM), glycerol (434 mM) and sodium tetraborate (10 mM), where the concentrations of each components are given in the parenthesis.

M= PVA, Dextrose, Glycerol and C16EMorphBr ; S= Sodium tetraborate.
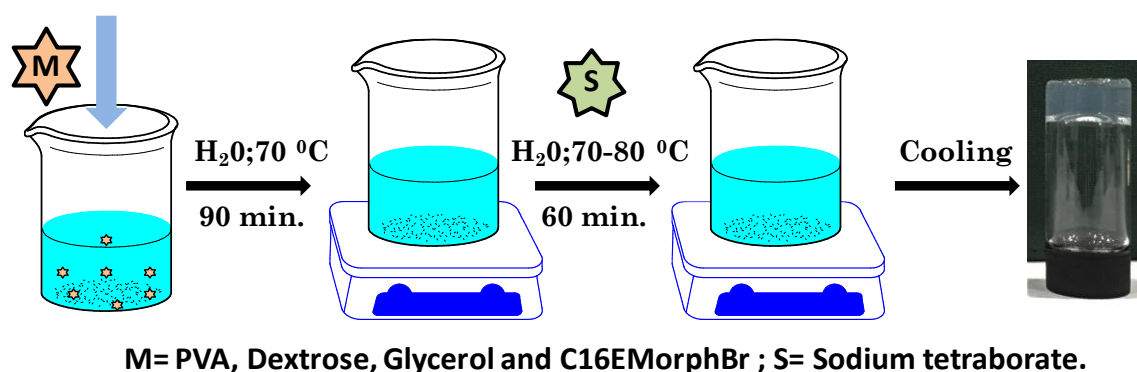
Scheme 2. Schematic representation for the hydrogel preparation.

2.3 Fourier Transform Infrared Spectroscopy (FTIR)

The FTIR spectra of PVA + H_2O, PVA + C_{16}EMorphBr + dextrose + H_2O and PVA + C_{16}EMorphBr + dextrose + glycerol +sodium tetraborate + H_2O were recorded using a Shimadzu FTIR-8400S spectrophotometer to deduce the possible interactions between the molecules or with the solvent.

2.4 Dynamic light scattering (DLS) and zeta potential measurement

DLS measurements were carried out in a Zetasizer nano ZS (Malvern, UK) by varying pH and temperature of the polymeric hydrogel. Same instrument was used to measure the zeta potential of polymeric hydrogel using a dip cell.

2.5   Small-angle neutron scattering (SANS)

Small-angle neutron scattering experiments were performed at 25 and 37 °C using the SANS-I diffractometer at Guide Tube Laboratory, Dhruva Reactor, Bhabha Atomic Research Centre, Mumbai, India.[18] SAS Fit analyzing software was used here to analyze the experimental scattering data using different fitting models.

Equations (i) and (ii) were used to get the output of the 1D scattering intensity function for cylinders:

$$P(q) = \frac{Scale}{V} N \int_0^{\pi/2} F^2(q,a) . \sin a \, da + background \qquad (i)$$

With

$$F(q,a) = 2(\Delta\rho)V \frac{\sin\left(\frac{1}{2} qL \cos a\right)}{\frac{1}{2} qL \cos a} \frac{J_1 (qR \sin a)}{qR \sin a} \qquad (ii)$$

Where a, q and Δρ are the angle between the axis of the cylinder, the volume of the cylinder and scattering length density differences between the scatterer and the solvent respectively whereas J_1 is the first order Bessel function.

2.6   Morphology of the hydrogel

The morphology of the hydrogel was studied using SEM (Hitachi S-3400 N), FE-SEM (Hitachi S-4800), TEM (Philips CM-200), and AFM (Park XE 100) using previously reported methods.[28]

2.7   Rheology

Rheological analysis was carried out on a Physica MCR 301 (Anton Paar) rheometer at 25 °C. We have used a 40 mm-diameter parallel plate (1 mm gap)

that is attached to a transducer. We have placed the polymeric hydrogel sample between the parallel plates while taking care of solvent from evaporation. Angular frequency sweep measurement was performed at 1-100 rad s^{-1} under a constant strain of 0.1%. These rheological measurements were perfromed within the viscoelastic region where G' and G" are storage and loss modulus and are independent of strain amplitude. Frequency was fixed to 1 rad s^{-1} while performing the strain scans from 0.1 to 10%. The critical strain was defined as the point from where G' and G" crosses over, which results in gel breakdown. The polymeric hydrogel was tested for its self- recovery properties against the applied shear forces through measuring the strain sweep or thixotropic properties of the hydrogel. Frequency was fixed to 1.0 Hz when the strain was changed from 0.1% to 25%.

2.8   Adhesiveness of the polymeric hydrogels

The adhesive properties were measured by lap-shear strength tests on different samples such as rubber, porcine skin, and glass. Briefly, after cutting the sample into fragments (35 mm × 10 mm), freshly prepared hydrogel (100 µl) was applied to one of the fragments. Second fragment of the sample was then brought in contact with the first one. The contact area between the sample and hydrogel was chosen to be 10 × 10 mm^2. After applying a 50 g/cm^2 load for 6.0 h, the adhesion strength was measured using a Testometric M100-1CT instrument.

2.9   Dynamic Swelling behavior of hydrogel

Accurately weighed hydrogel samples were immersed separately in aqueous buffer solution of 10 mL at pH 7.4 and pH 5 (at 37 ^{0}C) for 2 h to attain the swelling equilibrium. At pre-determined time, the hydrogel samples were taken out and weighed. Surface water was removed using the tissue paper and the weight of the swollen gel (W_X) was determined. The equilibrium-swelling ratio (Q) of the hydrogel was calculated from equation (iii):

$$Q = \frac{W_a}{W_b} \tag{iii}$$

Where, W_a is the weight of water molecules in the swollen 3D gel network under certain condition and W_b is the weight of the dry gel.

2.10 Phase Transition Behavior

The gel-to-sol transition of hydrogels (pH=5.0; pH=7.4) were confirmed using Cary 50 UV/visible spectrometer within the temperature range of 20 to 90 °C. Temperature was controlled using peltier-controlled variable temperature cell holder.

2.11 *In vitro* degradation of gel.

The degradation of polymeric hydrogel was investigated using phosphate buffered saline (PBS) solution with pH 7.4 (normal tissue) and pH 5 (cancerous tumour tissues). The hydrogel was weighed accurately and immersed into the buffer solution of choice. The mixture was then stirred magnetically (50-70 rpm) before placing the gel samples in incubation for 42 days at 37 °C. The degradation of the hydrogel was observed through measuring the change in weight of the gel at regular time intervals using equation (iv):

$$\text{Loss of mass (\%)} = \frac{M_x - M_y}{M_x} * 100 \qquad \text{(iv)}$$

Where, M_x and M_y are dry mass of the gel sample initially and after the certain time of degradation.

2.12 Drug Loading studies.

We used modified breathing-in mechanism to load DOX within the polymeric hydrogel (with and without $C_{16}EMorphBr$). The samples were than put on shaker for 3h followed by centrifugation at 10,000 rpm for 10 to 15 min. The supernatant obtained was diluted and the drug present in that was measured using UV-Vis spectrometer at 480-485 nm. Equations (v) and (vi) were used to calculate the drug loading efficiency (LE) and encapsulation efficiencies (EE):

$$LE\ (\%) = \frac{\text{Initial Drug Concentration} - \text{Drug Concentration After Loading}}{\text{Initial Drug Concentration}} * 100 \qquad \text{(v)}$$

$$EE\ (\%) = \frac{Loading\ Efficiency - \text{Initial Drug Concentration(µg/ml)}}{Initial\ Hydrogel\ concentration\ \text{(µg/ml)}} * 100 \qquad \text{(vi)}$$

2.13 *In vitro* DOX release studies.

To measure the effect of temperature and pH changes on DOX release, the drug loaded polymeric hydrogel was immersed in 37 °C, pH = 5.0 and 7.4 PBS at 200 rpm. At pre-determined time intervals, the drug release media were removed and replaced with fresh PBS. Absorbance at 480-485 nm was measured using Cary 50 UV/visible spectrometer to determine the amount of DOX in the release medium.

2.14 Cytotoxicity Assay (MCF-07 and HeLa cell)

The *in vitro* cytotoxicity of polymeric hydrogel and DOX-loaded hydrogel was performed through the 3-(4,5-dimethylthiazol-2-yl)-2,5-diphenyltetrazolium bromide (MTT) assay. The cell lines were selected were, MCF-7 (human breast cancer cell line) and HeLa (human ovarian cancer). Briefly, the cells were seeded in each well of the plates with 96-well, cultured overnight and exposed to successive concentrations of DOX free polymeric hydrogel and DOX loaded hydrogel (1, 5, 10 and 15 µg/mL DOX) in culture medium. Physiological temperature (37 °C) and 5% CO_2 incubator was selected to incubate the cell as the controls. The medium was removed once the cells were cultivated for 48 h. Subsequently; the cells were washed with PBS buffer with ultimate care and again incubated with fresh 5 mg/mL MTT medium for more 4 h. The cycle of removing the medium was repeated and 200 µL DMSO per well was added. The plates containing the cell wells were incubated at 37 °C for approximately 10 min and the absorbance was recorded at 540 nm using microplate readers. Cell viability was calculated with respect to positive and negative controls.

2.15 Drug uptake analysis

Cells were seeded 50,000 cells/well in 6-well plates and cultured until 70% confluency had been reached. After this time the media was replaced with varied concentrations of DOX loaded hydrogel in culture medium, respectively (DOX Free, 1 µg/mL DOX, 5 µg/mL DOX, 10 µg/mL DOX & 15 µg/mL DOX). The cells were cultured for 4 and 24 h after which the media was removed, and they were washed three times with phosphate buffered saline. The cells were counted and 100,000 cells aliquoted into an eppendorf tube. The cell suspension was centrifuged at 800 rpm, the supernatant removed, and cells suspended in water. The amount of DOX was measured using a UV-Vis spectrophotometer at 480-485 nm and calculated per cell, comparing to controls.

3.   Results and Discussion

We focused here to design a polymeric hydrogel based drug delivery vehicle that can be (i) programmed to release the encapsulated drug through biological stimuli (pH and temperature), (ii) capable of secondary modifications and (iii) is capable to retain high water to allow passive diffusion of the entrapped drug upon hydration. The designed PVA based hydrogel consists of C_{16}EMorphBr, dextrose, glycerol and sodium tetraborate as the additives, functions of which are already mentioned in the introduction section of the manuscript. The PVA based hydrogel possesses insufficient elastic properties; forms stiff membrane and offer limited hydrophilicity for the biomedical applications in its purest form.[29,30] Whereas, C_{16}EMorphBr based hydrogel though having known biodegradability and biocompatibility, have higher critical gelation concentration (CGC, 7.20 % w/v) and lack in mechanical strength, which restricts its commercial applications as the drug carrier.[27] To ameliorate this, herein, we had proposed the formation of PVA based hybrid hydrogel with C_{16}EMorphBr as an additive, where the ratio of mass fraction was 10:1 for PVA :C_{16}EMorphBr. Through addition of C_{16}EMorphBr, we aim to (i) control the cost and injectability of the hydrogel and (ii) improve the hydrophilicity of the hydrogel. We further added dextrose (x_i = 0.0025) to improve the mechanical properties of the hydrogel and glycerol (x_i = 0.000025) as well as sodium tetraborate (x_i = 0.0000038) to induce the self-healing property in the polymeric hybrid hydrogel. The polymeric solution was

transformed into hydrogel upon cooling due to the molecular interactions within the components of the mixture. The molecular interactions responsible for the sol-gel transition are confirmed through the change in the frequency within the FTIR spectrum of the components of the hydrogel and are shown in Figure 1A. The hybrid hydrogel was formed during the sol-gel transition in which Dextrose-C_{16}EMorphBr, Dextrose-PVA, and C_{16}EMorphBr-PVA were strongly cross linked (Figure 1B). Strong supporting hydrogen bonds are present between the Dextrose-C_{16}EMorphBr-PVA (H-bonding I) and reversible hydrogen bond link PVA-Borax-PVA to PVA-Glycerol-PVA (H-bonding II).[31] The movement of the PVA chains are restricted through these strong H-bonding network and exhibited a stimuli-free self-healing ability (Video-S1) to the polymeric hydrogel and improved its mechanical stability. These hydrogen bonds follows the bond strength in the order of: H-bonding I> H-bonding II.[31]

(A)   (B)
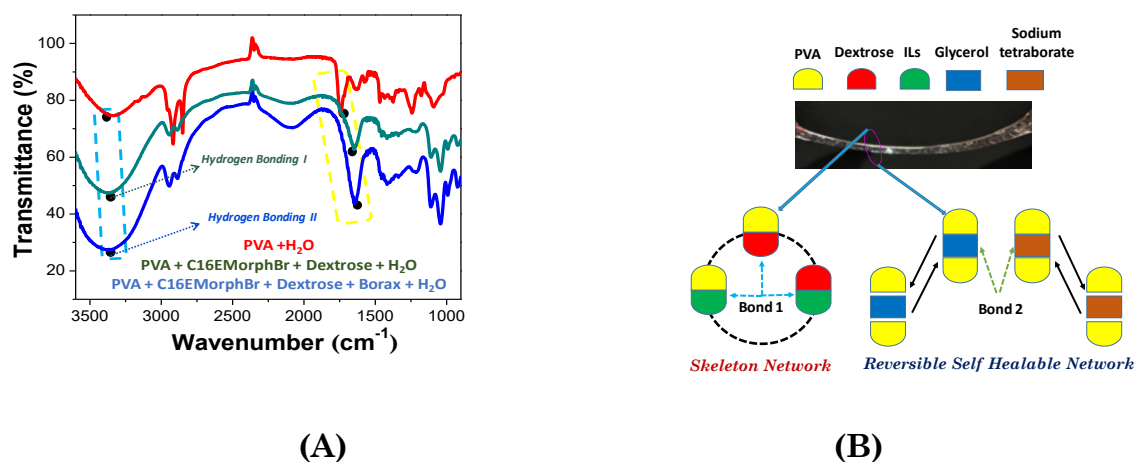
Figure 1.   (A) FT-IR spectra of hydrogel with different components; (B) Schematic representation of the internal structures and bonds of self-healable hydrogel.
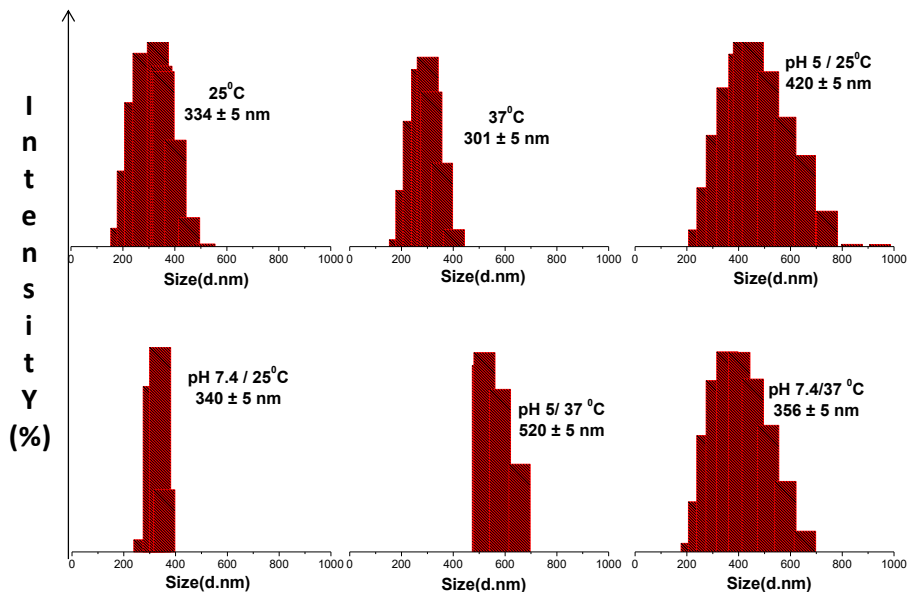
Figure 2. Temperature and pH responsive size distribution of polymeric hydrogels.

Table 1: Temperature and pH responsive size distribution of polymeric hydrogels.

Gel	Temperature ^{0}C		pH (25 ^{o}C)		pH (37 ^{o}C)	
	25	37	5	7.4	5	7.4
Size	332 ±5	301±5	420±5	340±5	520±5	356±5
PDI	0.33	0.21	0.21	0.28	0.29	0.20
Zeta	-19	-20	-13	-18	-17	-11.5

To effectively use the hydrogel for drug delivery purpose, it is recommended to investigate whether the hydrogel the stimuli responsive. To counter this argument, we hereby studied the hydrodynamic sizes of the gelators within the hydrogel matrix through DLS under the influence of temperature and pH. The data also helps us to define the conditions for the drug encapsulation and release. The results of size distribution along with the distribution plots are

shown in Table 1 and Figure 2 respectively. Interestingly, out of the three hydrogel samples, hydrogel with 75 mL water (25 mL of sodium tetraborate; total amount of water (T_a) is 100 mL), showed increase in the size of the aggregates with increasing temperature, whereas rest of the hydrogels; 25 mL (T_a=50 mL) and 50 mL (T_a=75 mL) showed a non-specific response to temperature. Higher degree of cross-linking often renders a greater extent of rigidness and stiffness to the gel networks, which in turn restricts the temperature sensitivity of the hydrogel. In addition, below 37 ℃ the hydrogel was in more hydrated form and show maximum swelling state with size of the aggregates in the range of 332 ± 5 nm at 25 ℃. Further, as the temperature increases to 37 ℃, the size of the aggregates within the hydrogel matrix decreases to 301 ± 5 nm (Figure 2), possibly because of water exclusion from the hydration shell. This eventually resulted in the collapse of the hydrogel due to volume phase transition (VPT) and resulted in a more compact gel networks because of the increased hydrophobicity. [32,33] It is worth to mention here that PDI values decreases with temperature (0.33 at 25 ℃ and 0.21 at 37 ℃), indicative of the phase transition (Table 1). Further, zeta potential data exhibited minor increase in the surface charge from -19 to -20 mV across the temperature range that indicates the increased colloidal stability with temperature.[34]

Temperature and pH affects inversely on the size of aggregates within the polymeric hydrogel. The interplay of forces responsible for swelling of the polymeric hydrogel are certainly responsible for the changes observed at higher temperature and acidic pH (Figure 2). At acidic pH, the hydrogel gets protonated and attracts higher amount of water molecules on its surface through H-bonding and increases the size of the aggregates. Higher degree of swelling at acid pH further strengthen the claim, *vide infra*. It was found that polymeric hydrogel exhibited temperature and pH responsive characteristics with optimum size at 37 ℃ and 5.0 pH (Table 1). Other formulations (25 ℃ and 5.0 pH, 37 ℃ and 7.4 and 25 ℃ and 7.4 pH) that are tested in the present work did not show any particular trend. These data are the basis of our drug encapsulation and release of the entrapped drug from the polymeric hydrogel system studied here.

We further employed small angle neutron scattering (SANS) to verify the effect of pH and temperature on the size of the aggregates within hydrogel matrix. In the SANS experiment, we measure the differential scattering cross section (dΣ/dΩ) per unit volume as a function of wave vector transfer (q). As shown in Figure 3, all the data were fitted using (q^{-1}) cylindrical micellar model.[27,35,36] With increasing the temperature and decreasing the pH of the gel system (from 25 to 37 ^{o}C and 7.4 to 5.0 pH), the cross-sectional radius of the cylinder increases. This implies that the radius of aggregates increases with increasing the temperature and decreasing the pH, also evidenced by DLS measurements, *vide supra* (Table 2).

Table 2: Fitted parameters from modeling of SANS experimental.

| *Parameters* *(Cylindrical micelles)*	Without drug (pH 7.4)		pH (25 ^{o}C)		pH (37 ^{o}C)	
	25 ^{o}C	*37 ^{o}C*	*5.0*	*7.4*	*5.0*	*7.4*
Cross-sectional radius (Å)	19.0	21.2	25.0	24.2	25.1	24.8
Length (L)	> 350 Å					
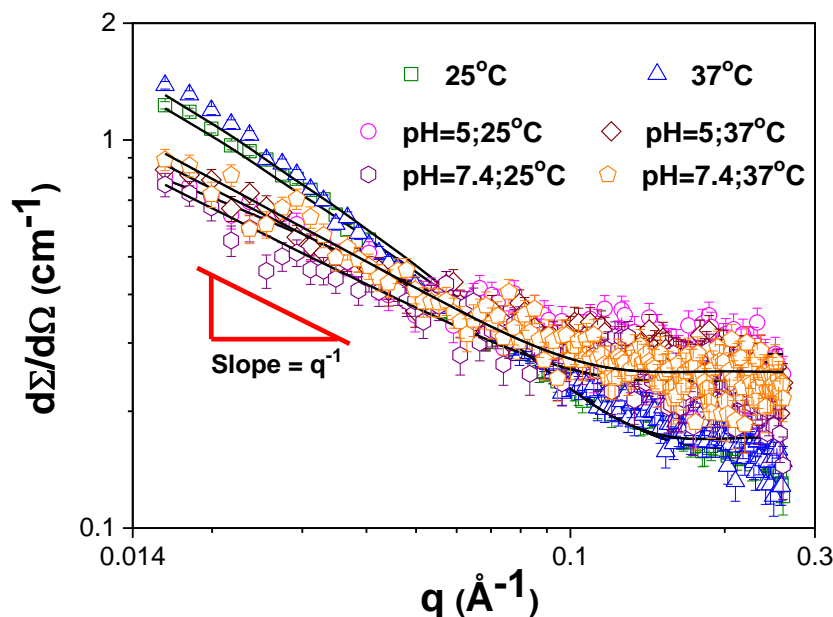
**Figure 3**: SANS scattering of hydrogel samples at various temperatures and pH.

The structural arrangement within the hydrogel has been explored through studying the morphology. We studied the morphology of the hydrogel through SEM, FE-SEM, TEM, and AFM imaging. Figure 4A presents a typical SEM image, showcasing the hierarchical porous three dimensional (3D) structure with smooth and porous structure with an irregular distribution of micro and nanometer scale pores.[26] FE-SEM image was acquired to reveal the 3D fibrous structures and assembly in the hydrogel which are composed of fibers with diameters < 20 μm (Figure 4B).[28] TEM images confirmed that the 3D hydrogel was formed through ordered fibers ranging in the length of 100 nm (Figure 4C).[37] Further, AFM (Figure 4D) image that is effective in providing surface topography and phase images confirmed the formation of a porous, soft and fibrous structure within the hydrogel. The AFM images of the polymeric hydrogel in Figure 4D show good agreement with the results of the SEM and FE-SEM studies.[38]
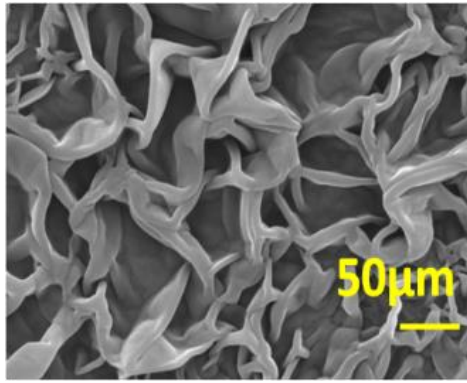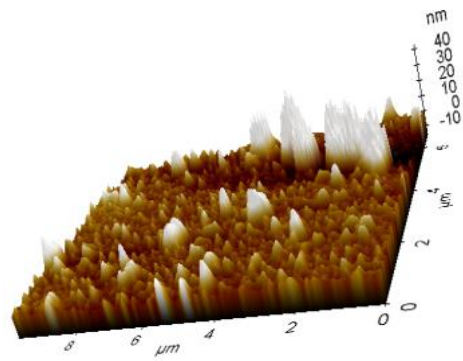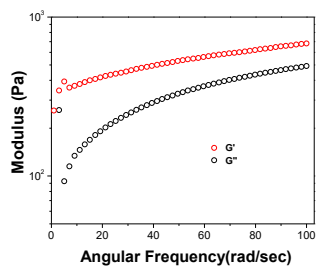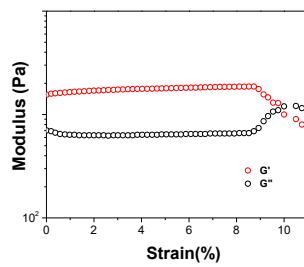
(A)
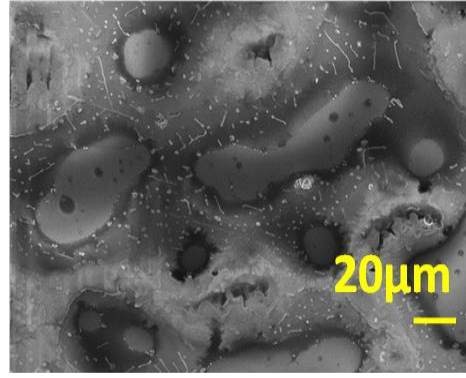
(B)
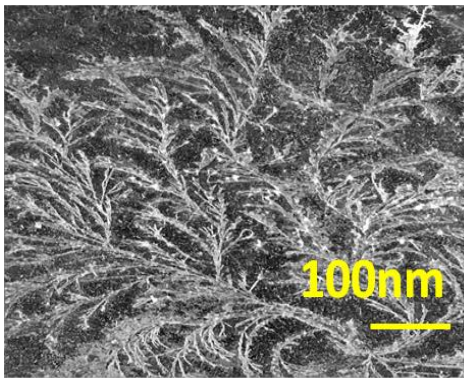
(C)

(D)

Figure 4. Morphology of the hydrogel through (A) SEM; (B) FESEM; (C) TEM; and (D) AFM images.

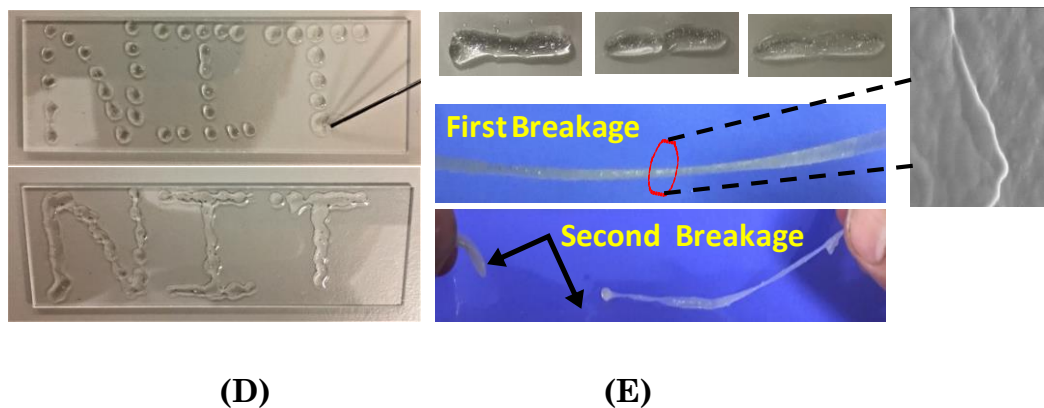
(A)

(B)

(C)

(D)   **(E)**
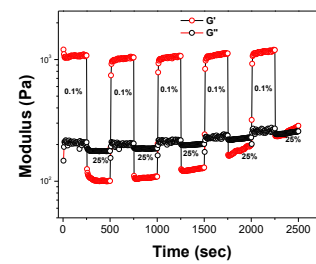
Figure 5.   (A) Frequency sweep dynamic rheology data at 25 °C (strain 0.1%);
(B) Strain sweep dynamic rheological data for the hydrogel 25°C (ω
= 1 rad s^{-1}); (C) Thixotropic data of the gel, obtained by step-strain
measurements at 25 °C at a constant frequency (1 rad s^{-1}); (D) 'NIT'
letter written through syringe to showcase the self-healing
character of hydrogel; (E) Self-healing properties and SEM image of
self-repaired previously damaged location after the hydrogel
underwent self-healing.

The strain sweep and angular frequency sweep measurements were performed for the polymeric hydrogel to explore its mechanical strength.[27,28,35] The changes in the storage moduli G', and loss moduli G", as a function of angular frequency for the polymeric hydrogel at 25 °C is shown in Figure 5A. It can be seen that at fixed strain of 0.1%, G' was higher than G" within the whole frequency range, which indicates the unstable colloidal particles that forms 3D branched solid-like network within the hydrogel, SEM image, *vide infra*. The strain amplitude sweep of the hydrogel sample (Figure 5B) demonstrated the elastic response typical of polymeric hydrogel.[39] Rapid decrease in G' was observed beyond the critical strain strain value (γ_c), i.e. 8.5% and the cross-over was observed at 9.8% strain. Above γ_c, G' decreases through breaking of the 3D network within the hydrogel. We note that the mechanical properties of the studied hydrogel exhibits rapid recovery after a large amplitude oscillatory breakdown, also known as thixotropic behavior of the hydrogel (Figure 5C).[15,40] Under the application of a large amplitude oscillatory force (= 25%; =0.1 rad s^{-1}), the G' decreases from 1205 to 110.6 Pa, resulting in a quasi-liquid state of the

hydrogel (tan δ=1.69). However, when the amplitude is decreased (= 0.1%; =0.1 rad s^{-1}), immediate recovery in G' to its initial value was observed and it return to quasi-solid state (tan δ= 0.12).[41]

According to the results for rheological recovery properties (Figure 5C), the self-healable hydrogel studied here existed in a sol state under high shear strain and come back to the elastic (gel) state once the stress was removed. Therefore, this hydrogel could be used as an injectable gel through embedding the drugs within the gel matrix for localized treatments. The shear strain should be within the range of compressed plunger of the syringe through which the gel is passed and made to gel "flow" like liquid and pass through the needle. Herein, reported hydrogel was tested for its injectable properties and the hydrogel due to the dissociation of hydrogen bonding network mentioned above flow like liquid from the needle of the syringe (Figure 5D) merely by applying pressure through plunger. Once the pressure was removed, the extruded hydrogel returned to the gel state. The self-healing property of the polymeric hydrogel was explored through drawing the three letters 'NIT' (The initial letters of National Institute of Technology) in the fragments (Figure 5D) using the syringe. It was observed that without any external stimuli, these fragments of hydrogel became smoother (under ambient temperature) to complete the word 'NIT', exhibiting the excellent self-healing ability of the studied polymeric hydrogel.

In addition, the studied polymeric hydrogel was cut in pieces and allowed to self-repair without any external stimulus successfully (Figure 5E). It was further observed that the self-repaired hydrogel could be stretched more than 20 times than its original length without further breaking. After stretching beyond its limit the new damage was observed from the site other than its first healed site showcasing its excellent self-healing abilities.[31] These properties (self-healing and injectable behavior) of studied polymeric hydrogel could be envisaged as new age invasive strategy in delivering the drug and implant to the body.[15]

(A)

(B)

(C)
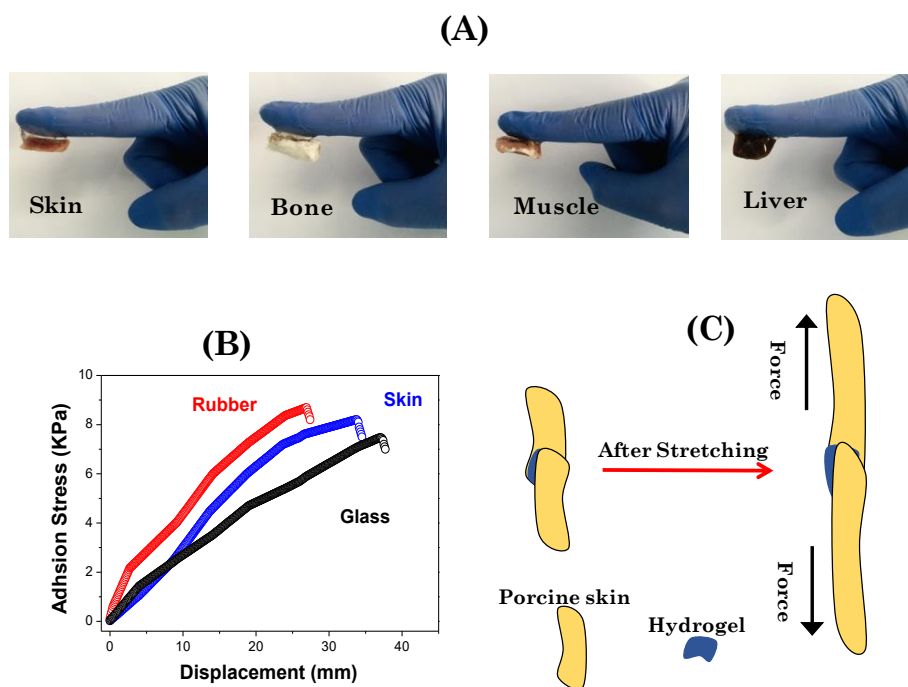
Figure 6. (A) Adhesion of the polymeric hydrogel with pig tissues, including skin, bone, muscle and liver; (B) Representative shear load–displacement curves of the polymeric hydrogels with different substrates; and (C) Schematic representation to determine the adhesive strength of the polymeric hydrogel on rubber, porcine skin and glass.

We have successfully explored the adhesive properties of the studied polymeric hydrogel with various biological tissues such as skin, fat, bone and muscle and the results in the form of visual images are given in Figure 6A. A schematic diagram (Figure 6C) illustrated the adhesive strength of the polymeric hydrogels to different substance (i.e. rubber, porcine skin, and glass). We used lab shear test to study the adhesion properties where 10 mm contact area was selected between the hydrogel sheet and the substrate. Here, the substrate was fixed and the polymeric hydrogel sheet was stretched at the controlled rate of 100 mm min^{-1}. Strongest adhesion was observed for the rubber samples. The adhesion stress as a function of displacement was drawn in order to get the adhesion strengths of the hydrogels with various substrates like porcine skin, glass and rubber (Figure 6B). Rubber due to it roughness provides the largest contact area with the hydrogel and showed the maximum value of the adhesion

stress of 8.68 KPa. Besides, the adhesion of polymeric hydrogels on porcine skin and glass are 8.20 KPa and 7.47 KPa respectively (Figure 6B). Present polymeric hydrogel offer higher adhesive behavior as compared to the various polymer-based gel; e.g. an ionic hydrogel with physically cross-linked polyvinyl alcohol demonstrated the values of 5.22 KPa.[42] In the polyacrylamide (AM) based hydrogel, the adhesive strength of the hydrogel to porcine skin was increased through doping AM with polydopamine (DA) and the adhesion strength was reached to its maximum (15.2 KPa) when the the ratio of DA to AM was 0.8 wt%.[43]
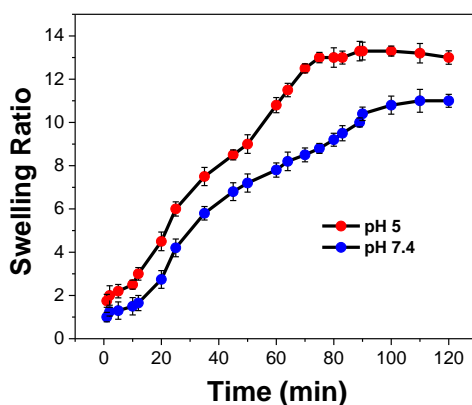

**Figure 7.**   Swelling kinetics of polymeric hydrogel at 37 °C.

Through studying the swelling kinetics of the hydrogel in aqueous medium, we determined the wettability of the hydrogel and the results are summarized in Figure 7. When the hydrogel was immersed in water, it readily absorbs water because of its highly porous 3D network structure. Results suggests that the hydrogel can absorbs water about ten times more than its weight on drying.[32,44] It takes approximately 70 ± 5 (pH =5) and 85 ± 5 min (pH =7.4) to attain the fully saturated state. As observed in Figure 7, swelling of the hydrogel was decreased at pH = 7.4, may be due to the presence of more physical crosslinks between 3D hydrogels network.[45]
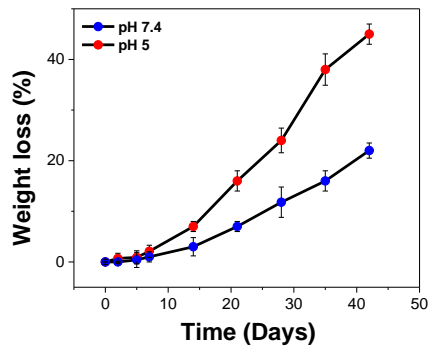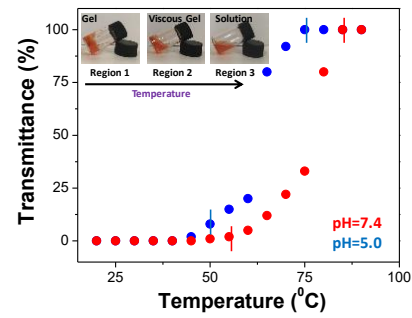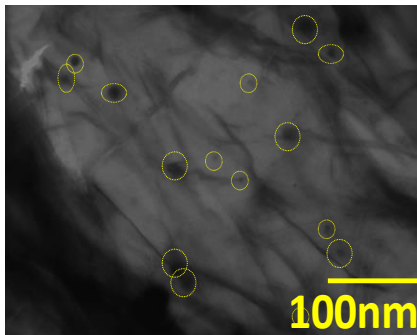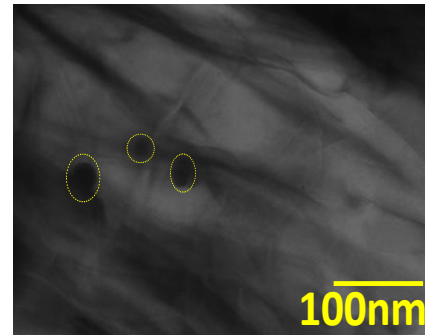
Figure 8. Degradation and *in vitro* release study (A) % weight loss of gel as a function of time when the hydrogel was incubated in pH 7.4 PBS and pH 5 PBS solution at 37 °C, (B) Phase transition of hydrogel (pH=5.0 and pH=7.4) at different temperatures, (C and D) TEM images of the DOX loaded polymeric hydrogel with and without C_{16}EMorphBr.

In order to utilize the hydrogel in implants, it is desirable to study its degradation behavior under the tumour cell and physiological conditions. This avoids the need for its surgical removal after the treatment and once the drug is released at its desirable rate. The *in vitro* biodegradation of hydrogel was estimated through observing the physical appearance of the hydrogel incubated under acidic (pH 5.0, the pH of tumour cells) and normal (pH 7.4) physiological condition. When incubated the hydrogel in the PBS buffer of 7.4, till 7 days no remarkable change in its physical appearance was observed (Figure 8A), after which we observed slight turbidity in the solution, indicating the degradation of the hydrogel. However, when incubated with pH 5.0 PBS, within 5 days of

incubation, slight turbidity was observed, ascribed to the breakage of 3D structures in the hydrogel matrix suggesting the quicker erosion of the hydrogel in the acidic condition.

As shown in Figure 8B, the gel-to-sol transition might be divided in to three regions, at the temperature below 50 ^{o}C (pH=5.0) and 55 ^{o}C (pH=7.4), the hydrogel remains semi solid like behavior and non-flowing characteristics with almost zero transmittance value (region 1). With increasing the temperature between 50-65 ^{0}C for pH=5.0 and 55-80 ^{0}C for pH=7.4, the transmittance increases gradually, and the hydrogel transformed into viscous gel (region 2). As the temperature reached 65 ^{o}C (pH=5.0) and 80 ^{o}C (pH=7.4) or above, viscous gel become a transparent solution with no fibrous aggregates could be observed (region 3). Such a temperature and pH induced phase transition was reversible and is probably because of the association and disassociation of the hydrogen bonding between molecule-molecule when the temperature and pH were changed. The hydrogel in the absence of C_{16}EMorphBr, showed low encapsulation efficiency (~52.4%) and drug loading capacity (~3.2%) for DOX, whereas the addition of DOX at the same ratio in the presence of C_{16}EMorphBr displayed higher encapsulation ~ 79.7% with a drug loading capacity at ~ 12.3%. Drug encapsulation and loading efficiencies of the sodium alginate-based hydrogel was enhanced by the addition of cationic gemini surfactant.[46] Therefore, C_{16}EMorphBr was determined to be a suitable candidate to improve loading efficiencies. TEM images of the gel with and without C_{16}EMorphBr show clear difference in the encapsulation of DOX (Figure 8C, 8D). Increased hydrophobicity of the system due to the incorporation of the C_{16}EMorphBr within the hydrogel matrix might be the reason for the increased drug encapsulation and loading efficiencies, FTIR spectra *vide supra*. Drug might get encapsulated within the fibrous structures of the gel matrix more in the presence of C_{16}EMorphBr.
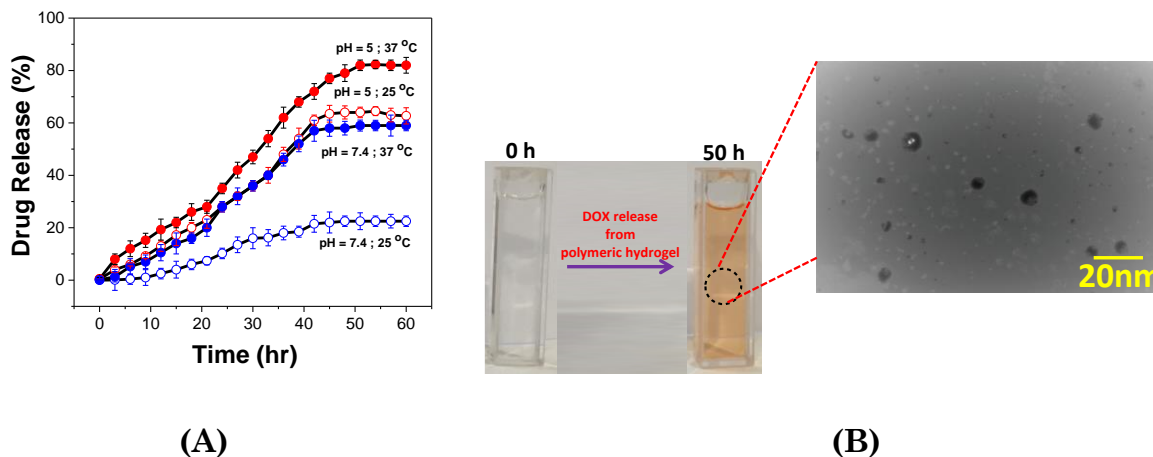
Figure 9: (A) Effect of temperature (25 °C and 37 °C) and pH (pH 5 and 7.4) on drug release kinetics; (B) DOX release from the polymeric hydrogel at 37 °C and pH 5.

Table 3: Statistical parameters derived through fitting the drug release data to zero order, first order and Higuchi model kinetic models;[47]

| Order	r^2@ pH (25 °C)		r^2 @ pH (37 °C)	
	7.4	5	7.4	5
Zero	0.874	0.921	0.893	0.902
First	0.810	0.889	0.963	0.921
Higuchi's	0.942	0.960	0.987	0.974

The *in-vitro* DOX release results under the two different physiological conditions of temperatures (25 °C and 37 °C) and pH (pH 5.0 and 7.4) from DOX loaded polymeric hydrogels are reported in Figure 9A. We observed ~82.3% cumulative release of DOX from the DOX loaded polymeric hydrogel at 37 °C and pH 5.0 after 50 h, whereas for the same time period ~53 % release was observed for pH 7.4. A similar pattern was observed when the polymeric hydrogel was incubated at 25 °C. The cumulative DOX release was ~64.0% at pH 5.0 and ~22.3% at pH 7.4. As expected, the acidic pH accelerate the release of DOX, attributed to the increased hydrophilicity of DOX and de-solubilization inside the

polymeric hydrogel fibrous network, thus drug release is enhanced. Further, more drug was released at 37 °C, likely due to the increased permeability within the hydrogel network.[48] Thus, the studied polymeric hydrogel demonstrate smart release of DOX controlled through temperature and pH. Comparing the above two conditions, we observed that DOX exhibited ~50% of sustained release in the former case while we observed only ~30% release in the latter case within 20 h. Above results demonstrate that the hydrogel studied here showed slow and sustained released of DOX under physiological conditions of temperature and (acidic) pH.[15,16,32] As shown in TEM image, drug molecules are released in PBS from the DOX loaded polymeric hydrogel at pH 5 and 37 °C (Figure 9B).

To get insights into the drug release mechanism, the *in vitro* release data were fitted to zero order equation, first order equation and Higuchi release kinetic models through plotting C_t vs t, log (C_0-C_t) vs t and C_t vs square root of t, respectively.[47] Here C_0 and C_t are the initial amount of drug in the hydrogel matrix and drug released at time t. It was concluded from the data of Table 3 that the DOX release from the hydrogel matrix were found to follow Higuchi release model.[49] The release of drug from gel occurs mainly through surface erosion. Influence of temperature and pH in changing the surface area and size of the aggregates also contributes to the release of the drug from the gel matrix.

We had assessed the cytotoxicity of polymeric hydrogel and DOX loaded polymeric hydrogel through treating the HeLa and MCF-7 cell lines with them. The polymeric hydrogel displayed excellent biocompatibility (Figure 10A, 10B) while DOX loaded- polymeric hydrogels exhibited higher toxicity as compare to the free DOX in cervical and breast cancer cell lines. Further, we used GraphPad Prism Software to determine the IC_{50} values from the dose response curve for DOX loaded polymeric hydrogels against MCF-7 cell lines and the results are summarized in Figure 10A and 10B. Regardless of incubation time, no-DOX polymeric hydrogels showed little to no cytotoxicity (Figure 10A, 10B). This shows that our system is a safe drug delivery method. The IC_{50} value in case of DOX loaded polymeric hydrogels for HeLa and MCF-7 cells were found to be 0.97 and 0.84 ± 0.5 μg/mL at 48h of the treatment exposure.
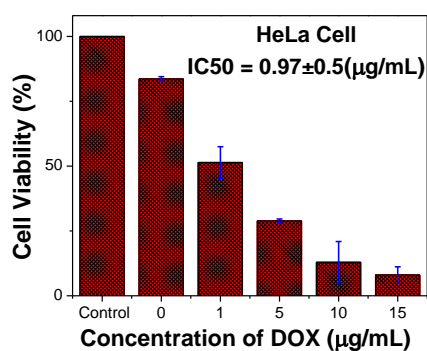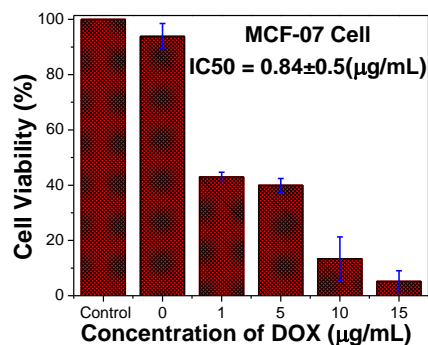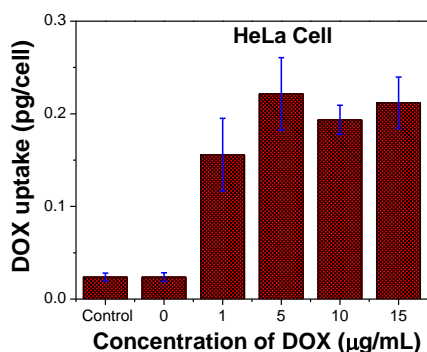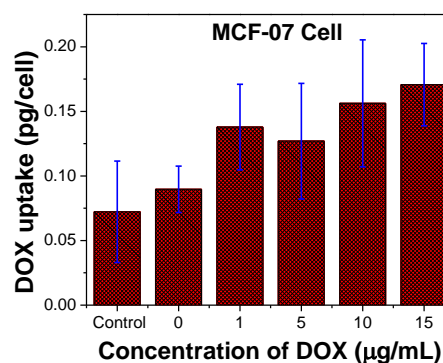
Figure 10. Cytotoxicity study. % cell viability of (A) HeLa and (B) MCF-7; Drug uptake study of (C) HeLa and (D) MCF-7 cells after exposure to different doses of DOX loaded polymeric hydrogels for 48 hrs.

Cellular uptake studies were performed to assess whether inclusion in the hydrogel influenced the drug ability to traffic into cells. The data (Figure 10C, 10D) showed that drug entered both cell lines in the picogram quantity per cell. In both cell lines, the data did not appear to show a concentration dependent uptake effect, possibly for these cells time is more influential in uptake. Indeed, DOX has been shown to take up to 48 h to internalize into cells in its native form, so the presence of the gel appears to be promoting earlier uptake, this finding rationalizes the cytotoxicity data, whereby, earlier uptake is resulting in greater cytotoxicity compared to the literature IC_{50} values.

4. Conclusion.

To sum up, we developed a pH and temperature dual responsive smart polymeric hydrogel as an efficient anticancer drug carrier. The drug release profile was dictated through measuring the swelling and phase transition behavior of the hydrogel at physiological conditions (37 ^{0}C and pH 5.0). DOX doped polymeric hydrogels exhibited improved encapsulation, cytotoxicity and drug uptake towards HeLa and MCF-7 cell lines. The dual stimuli responsive nature of the studied smart polymeric hydrogel could be envisaged as the smart drug carrier for the wide-ranging positively charged drugs for cancer therapy. In order to further elucidate this potential, further work is required in order to understand the in vitro trafficking mechanisms as well as drug localization within the cell, biodegradation in vitro and if favorable an *in vivo* efficacy study.

Supporting Information. Video description of the stimuli-free self-healing ability to the polymeric hydrogel is given as Video-S1.

References

1. https://www.who.int/news-room/fact-sheets/detail/cancer. Assessed on 13.06.2020.

2. Siegel, RL.; Miller, KD.; Jemal. A. Cancer statistics, 2016. *CA Cancer J. Clin.* **2016**, *66*, 7–30. https://doi.org/10.3322/caac.21332.

3. Mehlen, P.; Puisieux, A. Metastasis: a question of life or death. *Nat. Rev. Cancer* **2006**, *6*, 449–458. https://doi.org/10.1038/nrc1886.

4. Korfel, A.; Höcht, S.; Thiel, E. Combined and sequential systemic chemotherapy and radiotherapy for treatment of brain metastases. *Onkologey* **2008**, *14*, 255–259. https://doi.org/10.1007/s00761-008-1318-0.

5. Mei, L.; Xu, K.; Zhai, Z.; He, S.; Zhau, T.; Zhong, W. Doxorubicin-reinforced supramolecular hydrogels of RGD-derived peptide conjugates for pH responsive drug delivery. *Org. Biomol. Chem*. **2019,** *17*, 3853–3860. https://doi.org/10.1039/C9OB00046A.

6. Shen, W.; Chen, X.; Luan, J.; Wang, D.; Yu, L.; Ding, J. Sustained Co delivery of Cisplatin and Paclitaxel via an Injectable Prodrug Hydrogel for Ovarian Cancer Treatment. *ACS Appl. Mater. Interfaces* **2017**, *9* (46), 4003140046. https://doi.org/10.1021/acsami.7b11998.

7. Hua, S.; de Matos, M. B. C.; Metselaar, J. M.; Storm, G. Current Trends and Challenges in the Clinical Translation of Nanoparticulate Nanomedicines: Pathways for Translational Development and Commercialization. *Front. Pharmacol.* **2018**, *9*, 1–14.https://doi.org/10.3389/fphar.2018.00790.

8. Xin, Y.; Yin, M.; Zhao, L.; Meng, F.; Luo, L. Recent Progress on Nanoparticle-Based Drug Delivery Systems for Cancer Therapy. *Cancer Biol. Med.* **2017**, *14* (3), 228. https://doi.org/10.20892/j.issn.2095-3941.2017.0052.

9. Zheng, Y.; Cheng, Y.; Chen, J.; Ding, J.; Li, M.; Li, C.; Wang, J. C.; Chen, X. Injectable Hydrogel-Microsphere Construct with Sequential Degradation for Locally Synergistic Chemotherapy. *ACS Appl. Mater. Interfaces* **2017**, *9* (4), 3487–3496. https://doi.org/10.1021/acsami.6b15245.

10. Davidorf, F. H.; Chambers, R. B.; Kwon, O. W.; Doyle, W.; Gresak, P.; Frank, S. G. Ocular toxicity of vitrealpluronic polyol F-127. *Retina* **1990**, *10* (4), 297-300. https://doi.org/ 10.1097/00006982-199010000-00013.

11. Li, J.; Mooney, D. J. Designing Hydrogels for Controlled Drug Delivery. *Nat. Rev. Mater.* **2016**, *1* (12), 1–18. https://doi.org/10.1038/natrevmats.2016.71.

12. Van De Wetering, P.; Metters, A. T.; Schoenmakers, R. G.; Hubbell, J. A. Poly(Ethylene Glycol) Hydrogels Formed by Conjugate Addition with Controllable Swelling, Degradation, and Release of Pharmaceutically Active

Proteins. *J. Control. Release* **2005**, *102* (3), 619–627. https://doi.org/10.1016/j.jconrel.2004.10.029.

13. Qu, Y.; Chu, B. Y.; Peng, J. R.; Liao, J. F.; Qi, T. T.; Shi, K.; Zhang, X. N.; Wei, Y. Q.; Qian, Z. Y. A Biodegradable Thermo-Responsive Hybrid Hydrogel: Therapeutic Applications in Preventing the Post-Operative Recurrence of Breast Cancer. *NPG Asia Mater.* **2015**, *7* (8), 1–10. https://doi.org/10.1038/am.2015.83.

14. Cassano, R.; Mellace, S.; Pellegrino, M.; Ricchio, E.; Mauro, L.; Andò, S.; Picci, N.; Trombino, S. Biocompatible Targeting Hydrogels For Breast Cancer Treatment. *Mini. Rev. Med. Chem.* **2016**, *16* (8), 651-657. https://doi.org/10.2174/1389557515666150709104018.

15. Kuddushi, M.; Patel, N. K.; Rajput, S.; El Seoud, O. A.; Mata, J.; Malek, N. I.Temperature Responsive Low Molecular Weight Ionic Liquid Based Gelator: An Approach to Fabricate Anti-Cancer Drug Loaded Hybrid Ionogel. *ChemSystemsChem.* **2020**.https://doi.org/10.1002/syst.201900053R1.

16. Liu, H.; Shi, X.; Wu, D.; Kahsay Khshen, F.; Deng, L.; Dong, A.; Wang, W.; Zhang, J. Injectable, Biodegradable, Thermosensitive Nanoparticles-Aggregated Hydrogel with Tumor-Specific Targeting, Penetration, and Release for Efficient Postsurgical Prevention of Tumor Recurrence. *ACS Appl. Mater. Interfaces* **2019**, *11* (22), 19700–19711. https://doi.org/10.1021/acsami.9b01987.

17. Vaid, Z. S.; Rajput, S. M.; Kuddushi, M.; Kumar, A.; El Seoud, O. A.; Malek, N. I. Synergistic Interaction between Cholesterol and Functionalized Ionic Liquid Based Surfactant Leading to the Morphological Transition. *ChemistrySelect* **2018**, *3* (4), 1300–1308. https://doi.org/10.1002/slct.201702561.

18. Shah, A.; Kuddushi, M.; Ray, D.; Aswal, V. K.; Malek, N. I. Sodium Salicylate Mediated Ionic Liquid Based Catanionic Coacervates as Membrane-Free Microreactors for the Selective Sequestration of Dyes and Curcumin. *ChemSystemsChem* **2019**, *1900029*. https://doi.org/10.1002/syst.201900029.

19. Vaid, Z. S.; Kumar, A.; El Seoud, O. A.; Malek, N. I. Drug Induced Micelle-to-Vesicle Transition in Aqueous Solutions of Cationic Surfactants. *RSC Adv.* **2017**, *7* (7), 3861–3869. https://doi.org/10.1039/c6ra25577a.

20. Rajput, S. M.; Gangele, K.; Kumar, S.; Aswal, V. K. Nano-Vehicles for Drug Delivery Using Low-Cost Cationic Surfactants : A Drug Induced Structural Transitions. *ChemistrySelect,* **2018**, 9454–9463. https://doi.org/10.1002/slct.201801111.

21. Rajput, S. M.; Kumar, S.; Aswal, V. K.; El Seoud, O. A.; Malek, N. I.; Kailasa, S. K. Drug-Induced Micelle-to-Vesicle Transition of a Cationic Gemini Surfactant: Potential Applications in Drug Delivery. *ChemPhysChem* **2018**, *19* (7), 865–872. https://doi.org/10.1002/cphc.201701134.

22. Shah, A.; Kuddushi, M.; Rajput, S.; El Seoud, O. A.; Malek, N. I. Ionic Liquid-Based Catanionic Coacervates: Novel Microreactors for Membrane-Free Sequestration of Dyes and Curcumin. *ACS Omega* **2018**, *3* (12), 17751–17761. https://doi.org/10.1021/acsomega.8b02455.

23. Paradossi, G.; Cavalieri, F.; Chiessi, E.; Spagnoli, C.; Cowman, MK. Poly(vinyl alcohol) as versatile biomaterial for potential biomedical applications. *J. Mater. Sci. Mater. Med.* **2003**, *14* (8), 687-691. https://doi.org/10.1023/a:1024907615244.

24. Huang, H.; Qi, X.; Chen, Y.; Wu, Z. Thermo-Sensitive Hydrogels for Delivering Biotherapeutic Molecules: A Review. *Saudi Pharm. J.* **2019**, *27* (7), 990–997. https://doi.org/10.1016/j.jsps.2019.08.001.

25. Choi, Y. S.; Hong, S. R.; Lee, Y. M.; Song, K. W.; Park, M. H.; Nam, Y. S. Study on Gelatin-Containing Artificial Skin: I. Preparation and Characteristics of Novel Gelatin-Alginate Sponge. *Biomaterials* **1999**, *20* (5), 409–417. https://doi.org/10.1016/S0142-9612(98)00180-X.

26. Bhattarai, N.; Gunn, J.; Zhang, M. Chitosan-Based Hydrogels for Controlled, Localized Drug Delivery. *Adv. Drug Deliv. Rev.* **2010**, *62* (1), 83–99. https://doi.org/10.1016/j.addr.2009.07.019.

27. Kuddushi, M.; Rajput, S.; Shah, A.; Mata, J.; Aswal, V. K.; El Seoud, O.; Kumar, A.; Malek, N. I. Stimuli Responsive, Self-Sustainable, and Self-

Healable Functionalized Hydrogel with Dual Gelation, Load-Bearing, and Dye-Absorbing Properties. *ACS Appl. Mater. Interfaces* **2019**, *11* (21), 19572–19583. https://doi.org/10.1021/acsami.9b01129.

28. Kuddushi, M.; Patel, N. K.; Rajput, S.; Shah, A.; Seoud, O. A. El; Malek, N. I. Thermo-Switchable de Novo Ionic Liquid-Based Gelators with Dye-Absorbing and Drug-Encapsulating Characteristics. *ACS Omega* **2018**, *3*, 12068–12078. https://doi.org/10.1021/acsomega.8b01984.

29. Kumar, A.; Han, S. S. PVA-Based Hydrogels for Tissue Engineering: A Review. *Int. J. Polym. Mater. Polym. Biomater*. **2017**, 66 (4), 159–182. https://doi.org/10.1080/00914037.2016.1190930.

30. Sunaryono; Taufiq, A.; Mufti, N.; Hidayat, N.; Rugmai, S.; Soontaranon, S.; Putra, E. G. R.; Darminto. Analysis of Distribution of Polyvinyl Alcohol Hydrogel Nanocrystalline by Using SAXS Synchrotron. *IOP Conf. Ser. Mater. Sci. Eng.* **2017**, *202* (1) 012041-012050. https://doi.org/10.1088/1757-899X/202/1/012041.

31. Li, M.; Li, W.; Cai, W.; Zhang, X.; Wang, Z.; Street, J.; Ong, W. J.; Xia, Z.; Xu, Q. A Self-Healing Hydrogel with Pressure Sensitive Photoluminescence for Remote Force Measurement and Healing Assessment. *Mater. Horizons* **2019**, *6* (4), 703–710. https://doi.org/10.1039/c8mh01441h.

32. Verma, N. K.; Purohit, M. P.; Equbal, D.; Dhiman, N.; Singh, A.; Kar, A. K.; Shankar, J.; Tehlan, S.; Patnaik, S. Targeted Smart pH and Thermoresponsive N,O-Carboxymethyl Chitosan Conjugated Nanogels for Enhanced Therapeutic Efficacy of Doxorubicin in MCF-7 Breast Cancer Cells. *Bioconjug. Chem.* **2016**, *27* (11), 2605–2619. https://doi.org/10.1021/acs.bioconjchem.6b00366.

33. Pelton, R. H.; Chibante, P. Preparation of Aqueous Latices with N-Isopropylacrylamide. *Colloids and Surfaces* **1986**, *20* (3), 247–256. https://doi.org/10.1016/0166-6622(86)80274-8.

34. Wang, Z.; Yu, Y.; Dai, W.; Lu, J.; Cui, J.; Wu, H.; Yuan, L.; Zhang, H.; Wang, X.; Wang, J.; Zhang, X.; Zhang, Q. The Use of a Tumor Metastasis Targeting Peptide to Deliver Doxorubicin-Containing Liposomes to Highly Metastatic Cancer. *Biomaterials* **2012**, *33* (33), 8451–8460.

https://doi.org/10.1016/j.biomaterials.2012.08.031.

35. Kuddushi, M.; Mata, J.; Malek, N. Self-Sustainable, Self-Healable, Load Bearable and Moldable Stimuli Responsive Ionogel for the Selective Removal of Anionic Dyes from Aqueous Medium. *J. Mol. Liq.* **2019**, 112048. https://doi.org/10.1016/j.molliq.2019.112048.

36. Smith, C. L.; Mears, L. L. E.; Greeves, B. J.; Draper, E. R.; Doutch, J.; Adams, J.; Cowan, A. J. Gelation Enabled Charge Separation Following Visible Light Excitation Using Self-Assembled Perylene Bisimides. *Phys. Chem.Chem. Phys.* **2019**, 26466–26476. https://doi.org/10.1039/c9cp05839g.

37. Ilg, P. Stimuli-Responsive Hydrogels Cross-Linked by Magnetic Nanoparticles. *Soft Matter* **2013**, *9* (13), 3465–3468. https://doi.org/10.1039/c3sm27809c.

38. Belali, S.; Emandi, G.; Cafolla, A. A.; O'Connell, B.; Haffner, B.; Möbius, M. E.; Karimi, A.; Senge, M. O. Water-Soluble, Neutral 3,5-Diformyl-BODIPY with Extended Fluorescence Lifetime in a Self-Healable Chitosan Hydrogel. *Photochem. Photobiol. Sci.* **2017**, *16* (11), 1700–1708. https://doi.org/10.1039/c7pp00316a.

39. Lu, C.; Zhang, M.; Tang, D.; Yan, X.; Zhang, Z.; Zhou, Z.; Song, B.; Wang, H.; Li, X.; Yin, S.; Sepehrpour, H.; Stang, P. J. Fluorescent Metallacage-Core Supramolecular Polymer Gel Formed by Orthogonal Metal Coordination and Host-Guest Interactions. *J. Am. Chem. Soc.* **2018**, *140* (24), 7674–7680. https://doi.org/10.1021/jacs.8b03781.

40. Li, Z.; Zhang, Y. M.; Wang, H. Y.; Li, H.; Liu, Y. Mechanical Behaviors of Highly Swollen Supramolecular Hydrogels Mediated by Pseudorotaxanes. *Macromolecules* **2017**, *50* (3), 1141–1146. https://doi.org/10.1021/acs.macromol.6b02459.

41. Xie, W.; Gao,Q.; Guo, Z.; Wang, D.; Gao, F.; Wang, X.; Wei, Y.; Zhao, L. An Injectable and Self-Healing Thermo-Sensitive Magnetic Hydrogel for Asynchronous Control Release of Doxorubicin and Docetaxel to Treat Triple- Negative Breast Cancer. *ACS Appl. Mater. Interfaces* **2017** *9* (39), 33660-33673. https://doi.org/10.1021/acsami.7b10699.

42. Wnag, Z.; Chen, J.;Wang, L.; Gao, G.; Zhou, Y.; Wang, R.; Xu, T.; Yin, J.;Fu,

J. Flexible and wearable strain sensors based on tough and self-adhesive ion conducting hydrogels. *J. Mater. Chem.* B **2019**, *7*, 24-29. https://doi.org/10.1039/C8TB02629G.

43. Han, L.; Yan, L.; Wang, K.; Fang, L.; Zhang, H.; Tang, Y.; Ding, Y.; Weng, L. T.; Xu, J.; Weng, J.; Liu, T.; Ren, F.; Lu, X. Tough, Self-Healable and Tissue-Adhesive Hydrogel with Tunable Multifunctionality. *NPG Asia Mater.* **2017**, *9* (4). https://doi.org/10.1038/am.2017.33.

44. Sornkamnerd, S.; Okajima, M. K.; Kaneko, T. Tough and Porous Hydrogels Prepared by Simple Lyophilization of LC Gels. *ACS Omega* **2017**, *2* (8), 5304–5314. https://doi.org/10.1021/acsomega.7b00602.

45. Khan, S.; Anwar, N. Highly Porous pH-Responsive Carboxymethyl Chitosan- Grafted -Poly (Acrylic Acid) Based Smart Hydrogels for 5-Fluorouracil Controlled Delivery and Colon Targeting. *Int. J. Polym. Sci.* **2019**, *2019*, 1–15.https://doi.org/10.1155/2019/6579239.

46. Jabeen, S.; Chat, O. A.; Maswal, M.; Ashraf, U.; Rather, G. M.; Dar, A. A. Hydrogels of Sodium Alginate in Cationic Surfactants: Surfactant Dependent Modulation of Encapsulation/Release toward Ibuprofen. *Carbohydr. Polym.* **2015**, *133*, 144–153. https://doi.org/10.1016/j.carbpol.2015.06.111.

47. Higuchi, T. Mechanism of Sustained-action Medication. Theoretical Analysis of Rate of Release of Solid Drugs Dispersed in Solid Matrices. *J. Pharm. Sci.***1963**, *52* (12), 1145–1149. https://doi.org/10.1002/jps.2600521210.

48. Haghiralsadat, F.; Amoabediny, G.; Helder, M. N.; Naderinezhad, S.; Sheikhha, M. H.; Forouzanfar, T.; Zandieh-doulabi, B. A Comprehensive Mathematical Model of Drug Release Kinetics from Nano-Liposomes, Derived from Optimization Studies of Cationic PEGylated Liposomal Doxorubicin Formulations for Drug-Gene Delivery. *Artif. Cells, Nanomedicine Biotechnol.* **2018**, *46* (1), 169–177. https://doi.org/10.1080/21691401.2017.1304403.

49. Owonubi, S. J.; Aderibigbe, B. A.; Mukwevho, E.; Sadiku, E. R.; Ray, S. S. Characterization and in Vitro Release Kinetics of Antimalarials from Whey

Protein-Based Hydrogel Biocomposites. *Int. J. Ind. Chem.* **2018**, *9* (1), 39–52. https://doi.org/10.1007/s40090-018-0139-2.